


Communication

# Gram-Scale Synthesis of an Ultrastable Microporous Metal-Organic Framework for Efficient Adsorptive Separation of C<sub>2</sub>H<sub>2</sub>/CO<sub>2</sub> and C<sub>2</sub>H<sub>2</sub>/CH<sub>4</sub>

Nuo Xu <sup>1,†</sup>, Yunjia Jiang <sup>1,†</sup>, Wanqi Sun <sup>1</sup>, Jiahao Li <sup>1</sup>, Lingyao Wang <sup>1</sup>, Yujie Jin <sup>2</sup>, Yuanbin Zhang <sup>1,\*</sup>, Dongmei Wang <sup>1,\*</sup> and Simon Duttwyler <sup>2,\*</sup> 

<sup>1</sup> Key Laboratory of the Ministry of Education for Advanced Catalysis Materials, College of Chemistry and Life Sciences, Zhejiang Normal University, Jinhua 321004, China; Nuo\_Xu@zjnu.edu.cn (N.X.); Yunjia\_Jiang@zjnu.edu.cn (Y.J.); Wanqi\_Sun@zjnu.edu.cn (W.S.); 17857171863@zjnu.edu.cn (J.L.); lywang@zjnu.edu.cn (L.W.)

<sup>2</sup> Department of Chemistry, Yuquan Campus, Zhejiang University, 38 Zheda Road, Hangzhou 310027, China; 21837026@zju.edu.cn

\* Correspondence: ybzhang@zjnu.edu.cn (Y.Z.); dmwang@zjnu.edu.cn (D.W.); duttwyler@zju.edu.cn (S.D.)

† These authors contributed equally to this work.

**Abstract:** A highly water and thermally stable metal-organic framework (MOF) Zn<sub>2</sub>(Pydc)(Ata)<sub>2</sub> (**1**, H<sub>2</sub>Pydc = 3,5-pyridinedicarboxylic acid; HAta = 3-amino-1,2,4-triazole) was synthesized on a large scale using inexpensive commercially available ligands for efficient separation of C<sub>2</sub>H<sub>2</sub> from CH<sub>4</sub> and CO<sub>2</sub>. Compound **1** could take up 47.2 mL/g of C<sub>2</sub>H<sub>2</sub> under ambient conditions but only 33.0 mL/g of CO<sub>2</sub> and 19.1 mL/g of CH<sub>4</sub>. The calculated ideal absorbed solution theory (IAST) selectivities for equimolar C<sub>2</sub>H<sub>2</sub>/CO<sub>2</sub> and C<sub>2</sub>H<sub>2</sub>/CH<sub>4</sub> were 5.1 and 21.5, respectively, comparable to those many popular MOFs. The Q<sub>st</sub> values for C<sub>2</sub>H<sub>2</sub>, CO<sub>2</sub>, and CH<sub>4</sub> at a near-zero loading in **1** were 43.1, 32.1, and 22.5 kJ mol<sup>-1</sup>, respectively. The practical separation performance for C<sub>2</sub>H<sub>2</sub>/CO<sub>2</sub> mixtures was further confirmed by column breakthrough experiments.

**Keywords:** metal-organic frameworks; gas adsorption; C<sub>2</sub>H<sub>2</sub>/CO<sub>2</sub> separation; C<sub>2</sub>H<sub>2</sub>/CH<sub>4</sub> separation; gram-scale synthesis



**Citation:** Xu, N.; Jiang, Y.; Sun, W.; Li, J.; Wang, L.; Jin, Y.; Zhang, Y.; Wang, D.; Duttwyler, S. Gram-Scale Synthesis of an Ultrastable Microporous Metal-Organic Framework for Efficient Adsorptive Separation of C<sub>2</sub>H<sub>2</sub>/CO<sub>2</sub> and C<sub>2</sub>H<sub>2</sub>/CH<sub>4</sub>. *Molecules* **2021**, *26*, 5121. <https://doi.org/10.3390/molecules26175121>

Academic Editor: Gen Zhang

Received: 28 July 2021

Accepted: 23 August 2021

Published: 24 August 2021

**Publisher's Note:** MDPI stays neutral with regard to jurisdictional claims in published maps and institutional affiliations.



**Copyright:** © 2021 by the authors. Licensee MDPI, Basel, Switzerland. This article is an open access article distributed under the terms and conditions of the Creative Commons Attribution (CC BY) license (<https://creativecommons.org/licenses/by/4.0/>).

## 1. Introduction

Acetylene (C<sub>2</sub>H<sub>2</sub>) is one of most important fundamental chemicals in the petrochemical and electronic industries and is mainly produced by the cracking of petroleum or oxidative coupling of methane [1]. During such processes, some impurities like carbon dioxide (CO<sub>2</sub>) and methane (CH<sub>4</sub>) are cogenerated with C<sub>2</sub>H<sub>2</sub> and must be removed to improve the quality of the C<sub>2</sub>H<sub>2</sub> [2–4]. The traditional approaches for the separation of C<sub>2</sub>H<sub>2</sub>/CO<sub>2</sub> and C<sub>2</sub>H<sub>2</sub>/CH<sub>4</sub> based on cryogenic distillation or solvent extraction are either of high cost-/energy consumption or associated with pollution [5]. In this context, physisorptive separation using porous solid adsorbents has attracted particular interest due to the lower cost and energy penalty [6]. Among the diverse porous solid materials, metal-organic frameworks (MOFs) are of particular interest for such demands.

In the past decades, a large number of MOFs have been synthesized for various applications including but not limited to gas separation [7–17], carbon capture [18–22], pollutant removal [23,24], catalysis [25,26], sensing [27,28], energy devices [29,30], and water harvesting [31]. While many MOFs have shown remarkable separation selectivity for relatively distinct C<sub>2</sub>H<sub>2</sub> and CH<sub>4</sub>, it is still very challenging to separate C<sub>2</sub>H<sub>2</sub> and CO<sub>2</sub> due to their similar polarity, molecular shape and geometrical dimensions (3.32 × 3.34 × 5.70 Å<sup>3</sup> for C<sub>2</sub>H<sub>2</sub> vs. 3.18 × 3.33 × 5.36 Å<sup>3</sup> for CO<sub>2</sub>) [32–35]. Furthermore, most MOFs are sensitive to moisture, which renders them difficult to use under practical conditions where they are exposed to humidity [36]. Therefore, it is urgent to develop water and thermally stable

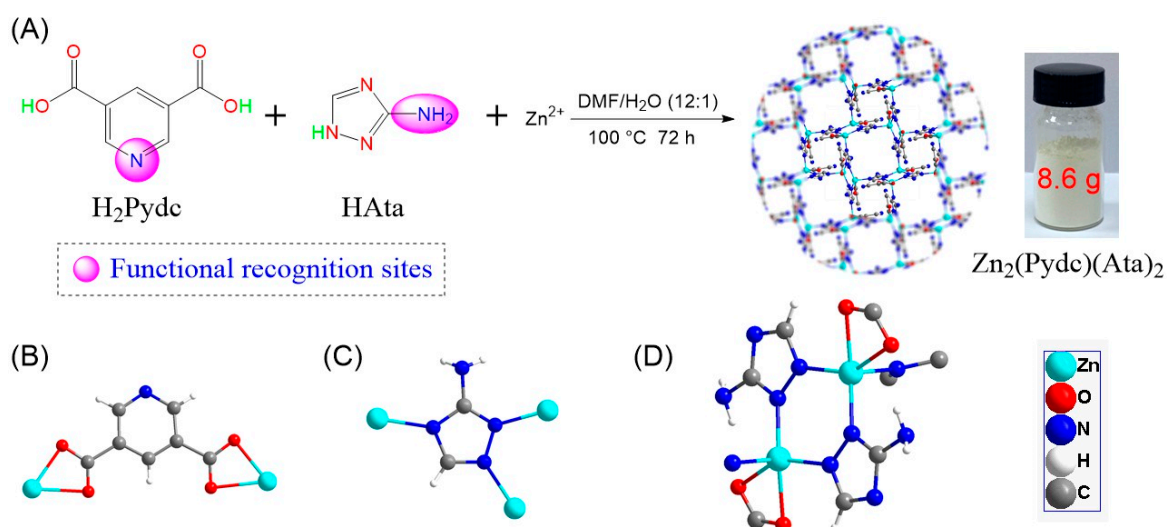
MOFs to facilitate the application of MOFs in gas separation. Besides, another important question that most chemists have neglected is that whether the MOFs can be synthesized on a large scale while maintaining the separation performance [37]. While a few hundred milligram samples are enough for characterization and property measurement in the laboratory, one-pot gram scale synthesis is necessary for practical use.

Herein, we would like to report a highly water and thermal stable MOF  $Zn_2(Pydc)(Ata)_2$  (**1**,  $H_2Pydc$  = 3,5-pyridinedicarboxylic acid;  $HAta$  = 3-amino-1,2,4-triazole) that is constructed by inexpensive commercially available ligands and zinc ions for efficient separation of  $C_2H_2$  from  $CH_4$  and  $CO_2$ . In our work, **1** was synthesized in a one-pot reaction in a flask with production of 8.6 g. PXRD patterns confirmed its pure phase with identical structures to that of small-scale synthesis in an autoclave. Static single component gas adsorption isotherms showed that **1** could take up  $54.9\text{ cm}^3/\text{g}$  of  $C_2H_2$  under 278 K and 1 bar, but only  $43.1\text{ cm}^3/\text{g}$  of  $CO_2$  and  $27.8\text{ cm}^3/\text{g}$  of  $CH_4$  under the same conditions. The selectivities calculated by ideal absorbed solution theory (IAST) were 5.1 and 21.5 for equimolar  $C_2H_2/CO_2$  and  $C_2H_2/CH_4$  mixtures, respectively. To confirm the practical separation performance of  $C_2H_2/CO_2$ , column breakthrough experiments were carried out for a  $C_2H_2/CO_2$  (50/50) mixture.  $CO_2$  broke out from the bed packed with **1** at 79 min while  $C_2H_2$  was retained in the column for 116 min, indicating the good dynamic separation performance of **1** for  $C_2H_2/CO_2$ .

## 2. Results and Discussion

The synthesis and crystal structure of  $Zn_2(Pydc)(Ata)_2$  (**1**) was first reported by Sun et al. [38]. Compound **1** features uncoordinated pyridyl and amino groups on the pore surface that can serve as recognition sites for interactions with guest molecules and is highly stable up to  $400\text{ }^\circ\text{C}$  and tolerant of acidic ( $\text{pH} \geq 2$ ) and basic ( $\text{pH} \leq 14$ ) aqueous solution conditions, which attracted our interest for the investigation of its application for selective gas separation. In the literature, **1** was synthesized on a very small scale (0.5 mmol) and the yield was specified. Although the stoichiometric ratio of  $Zn^{2+}:Pydc^{2-}:Ata^-$  in **1** is 2:1:2, the authors used a substrate ratio of 1:1:1 for the reaction. During the scale-up synthesis (34 mmol) of **1**, we found that the reported 1:1:1 substrate ratio was not reliable, as it led to a large amount of residual  $H_2Pydc$  and a huge reduction of yield. Once we used a  $Zn(NO_3)_2 \cdot 6H_2O:H_2Pydc:HAta = 2:1:2$  ratio, no  $H_2Pydc$  residue was observed and the yield was increased to 89% (Scheme 1A). The purity was confirmed by comparing the PXRD patterns of the as-synthesized powder and the one simulated from the single crystal structure (Figure S2). The single crystal structure of **1** revealed that it belongs to the tetragonal space group  $I4/m$ , exhibiting a 3D microporous framework. Two carboxylate groups from  $Pydc^{2-}$  are paired with two different  $Zn^{2+}$  ions, leaving the N sites free (Scheme 1B). For  $Ata^-$ , all three N atoms of the triazole ring are coordinated to three different  $Zn^{2+}$  ions while the  $-NH_2$  group is free (Scheme 1C). Looking at the coordination environment of the  $Zn^{2+}$  ion, one can find that a single  $Zn^{2+}$  ion is coordinated to two oxygen atoms and three nitrogen atoms (Scheme 1D).

Along the  $c$  axis, **1** features two different 1D channels characterized by  $Zn \cdots Zn$  distances of 6.135 and 5.914 Å (Figure 1A). However, the small channels are not accessible by guest molecules if the flexibility of the ligands is not considered, as indicated by the Connolly surface analysis which gives a Connolly radius of 1.2 Å (Figure 1B). The average diameter of the large channels decorated with electronegative nitrogen sites is 3.6 Å (Figure 1B,C), which is slightly larger than the kinetic diameter of  $C_2H_2$  (3.3 Å),  $CO_2$  (3.3 Å) but slightly smaller than that of  $CH_4$  (3.8 Å), thus suggesting its use as a potential material for selective  $C_2H_2/CO_2$  and  $C_2H_2/CH_4$ .



**Scheme 1.** (A) Synthetic route towards  $\text{Zn}_2(\text{Pydc})(\text{Ata})_2$ . (B)  $\text{Pydc}^{2-}$  coordination mode. (C)  $\text{Ata}^-$  coordination mode. (D)  $\text{Zn}^{2+}$  coordination environment.

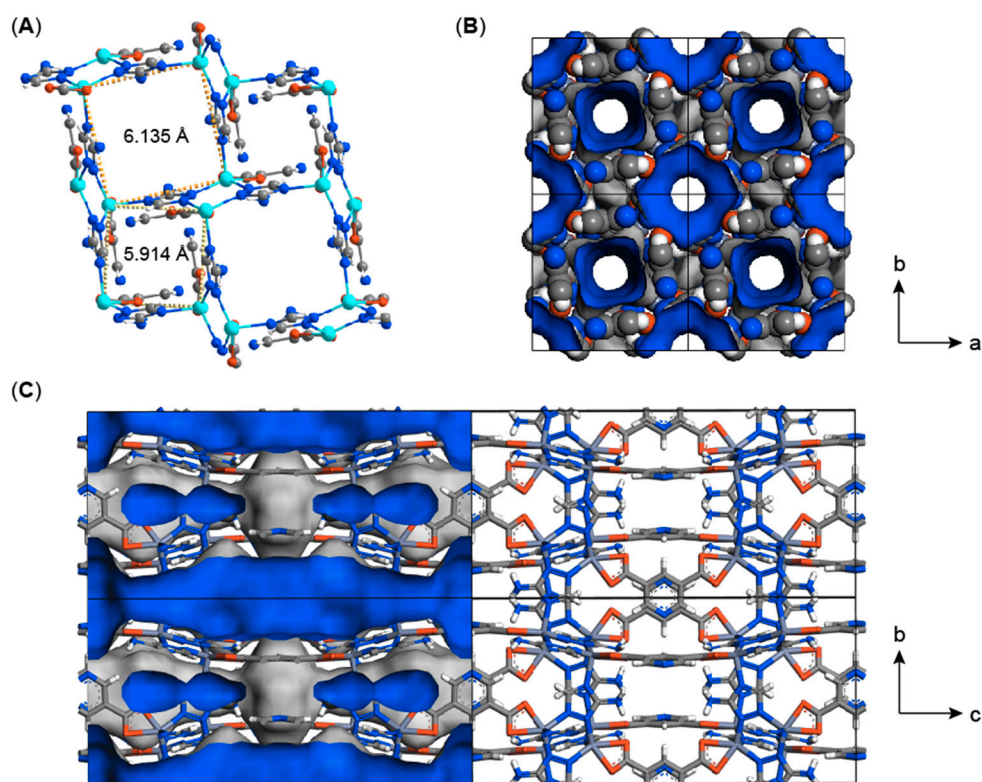


**Figure 1.** (A) Structure of **1** showing the 1D channel with two different dimensions. (B,C) Connolly isosurface mapping on **1**.

To explore the separation performance of **1**,  $\text{N}_2$  adsorption and desorption isotherms were first collected at 77 K after activation of **1** under vacuum at 200 °C for 12 h. Figure 2A shows that **1** could take up 153 mL/g of  $\text{N}_2$  at  $P/P_0 = 0.95$  and the adsorption isotherm belonged to typical type I. The pore volume and Brunauer-Emmett-Teller (BET) surface area were calculated to be 0.24  $\text{cm}^3/\text{g}$  and 636  $\text{m}^2/\text{g}$ , respectively, close to reported values for crystals [38]. Then,  $\text{C}_2\text{H}_2$ ,  $\text{CO}_2$ , and  $\text{CH}_4$  adsorption/desorption isotherms in **1** at 278 K, 288 K, and 298 K were collected, which all exhibited type I isotherms with negligible hysteresis (Figure 2B–D). The capacities of  $\text{C}_2\text{H}_2$ ,  $\text{CO}_2$ , and  $\text{CH}_4$  in **1** at 278 K were 54.9, 43.1, and 27.8 mL/g, respectively, which decreased to 52.6, 35.3, and 23.7 mL/g at 288

K and 47.2, 33.0, and 19.1 mL/g at 298 K. The isotherms were fitted using the dual-site Langmuir–Freundlich equation (Tables S1–S3), and the IAST (ideal absorbed solution theory) selectivities for equimolar  $C_2H_2/CO_2$  and  $C_2H_2/CH_4$  mixtures were calculated and shown in Figure 3A–C. For the  $C_2H_2/CO_2$  mixture, the IAST selectivities were 5.1, 5.3, and 3.9 under 278, 288, and 298 K at 100 kPa, which are comparable to those of many popular MOFs such as BSF-1 (3.3, 298 K) [39], ZJNU-109 (3.6, 288 K) [40], BSF-2 (5.1, 298 K) [41], UTSA-68 (3.4, 298 K) [42] as well as many others shown in Table 1. The IAST selectivities for the  $C_2H_2/CH_4$  mixture were much higher and the values were 21.5, 19.6, and 15.9 under 278, 288, and 298 K at 100 kPa, respectively. These good selectivities of  $C_2H_2$  over  $CO_2$  and  $CH_4$  originate from the higher affinity of **1** towards  $C_2H_2$  by  $N \cdots H-C$  hydrogen bonding. The IAST selectivities for  $C_2H_2/CO_2$  and  $C_2H_2/CH_4$  mixtures in **1** under 100 kPa with different  $C_2H_2$  ratios were also calculated, which indicated that the composition had a larger influence on the  $C_2H_2/CH_4$  mixture, but whether the influence was positive or negative depended on the temperature. At 298 and 278 K, the increasing  $C_2H_2$  ratio led to decreased selectivity while it decreased first and increased afterwards with the increase of the  $C_2H_2$  ratio at 288 K. The isosteric heats of adsorption ( $Q_{st}$ ) were calculated using the Clausius–Clapeyron equation.

The  $Q_{st}$  values for  $C_2H_2$ ,  $CO_2$ , and  $CH_4$  at a near-zero loading in **1** were calculated to be 43.1, 32.1, and 22.5  $\text{kJ mol}^{-1}$ , respectively (Figure 4A). These values were consistent with the adsorption isotherms showing that **1** accommodated  $C_2H_2$  more favorably than  $CO_2$  and  $CH_4$ .

To investigate its recyclability as well as regeneration conditions, cycling  $C_2H_2$  adsorption-desorption experiments were conducted on **1**. Figure 4B shows that **1** could be easily regenerated under vacuum at a mild temperature for 30 min. In detail, complete capacity could be realized under exposure to vacuum at temperatures above 50 °C for 30 min while >98% uptake was achieved under vacuum regeneration conditions at 25 °C for 30 min.

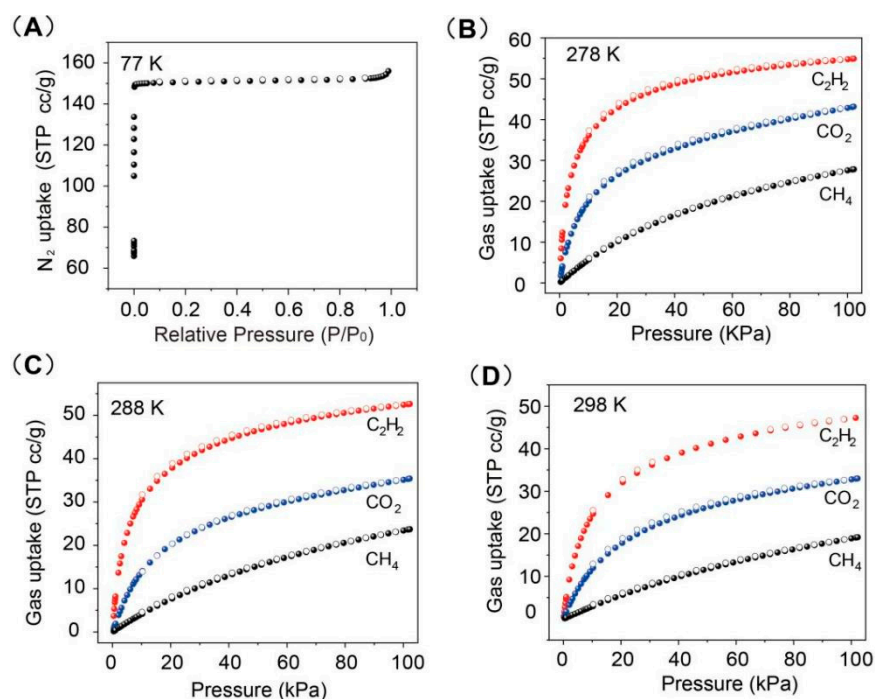


**Figure 2.** (A)  $N_2$  adsorption/desorption isotherms in **1** at 77 K. (B–D)  $C_2H_2$ ,  $CO_2$ , and  $CH_4$  adsorption/desorption isotherms in **1** at 278 K, 288 K, and 298 K.

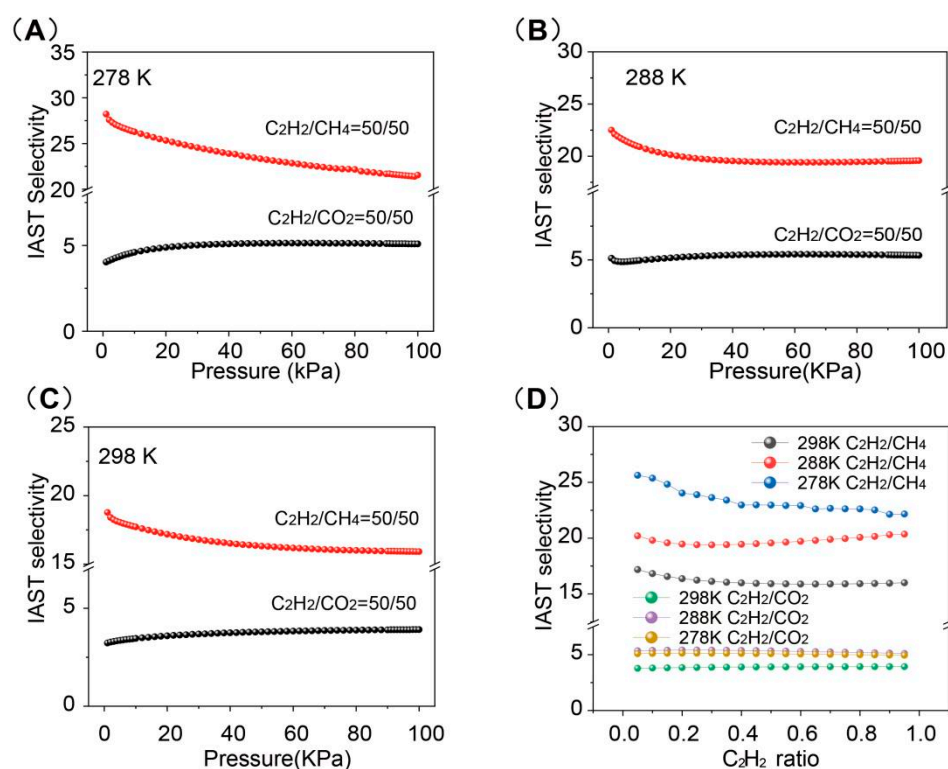


**Figure 3.** (A–C) IAST selectivities for equimolar C<sub>2</sub>H<sub>2</sub>/CO<sub>2</sub> and C<sub>2</sub>H<sub>2</sub>/CH<sub>4</sub> mixture in **1** at 278, 288, and 298 K. (D) IAST selectivities for C<sub>2</sub>H<sub>2</sub>/CO<sub>2</sub> and C<sub>2</sub>H<sub>2</sub>/CH<sub>4</sub> mixtures in **1** under 100 kPa with different C<sub>2</sub>H<sub>2</sub> ratio at 278, 288, and 298 K.

**Table 1.** Comparison of the gas adsorption performance of **1** and other MOFs.

	Uptake (cm <sup>3</sup> g <sup>-1</sup> ) (298 K, 100 kPa)			IAST Selectivity (298K, 100 kPa)		Ref
	C <sub>2</sub> H <sub>2</sub>	CO <sub>2</sub>	CH <sub>4</sub>	C <sub>2</sub> H <sub>2</sub> /CO <sub>2</sub>	C <sub>2</sub> H <sub>2</sub> /CH <sub>4</sub>	
FJI-C3	43.6	–	11.6	–	14.6	[43]
ZJNU-27	93.7	79.3	26.0	–	16.6	[44]
USTA-36	58.6 <sup>a</sup>	–	13.2 <sup>a</sup>	–	13.8 <sup>a</sup>	[45]
[Co <sub>3</sub> (L)(OH) <sub>2</sub> (H <sub>2</sub> O)]·2DMF·2H <sub>2</sub> O	107.3	62.0	17.7	–	13	[46]
QMOF-1	41.5	24.6	3.9	–	13.5	[47]
FJI-H21	92.4	–	7.10	–	16.3	[48]
JNU-1	63	51	–	3	–	[49]
JXNU-5a	55.9	34.8	–	5	–	[50]
UTSA-68	70.1 <sup>a</sup>	39.6 <sup>a</sup>	–	4 <sup>a</sup>	–	[42]
FJU-36a	52.2 <sup>a</sup>	35.5 <sup>a</sup>	10.5 <sup>a</sup>	2.8 <sup>a</sup>	17.7 <sup>a</sup>	[51]
BSF-1	52.5	39.7	10.5	3.3	46.9	[39]
BSF-2	41.5	29.7	5.4	5.1	324	[41]
BSF-3	81.8	47.3	13.4	16.3	205	[6]
ZNU-1 (BSF-9)	76.3	38.1	–	56.6	–	[52]
SNNU-63	91.1	43.7	10.3	3.3	12.9	[53]
ZJNU-109	104.6	60.0	14.3	3.8	21.6	[40]
Zn <sub>2</sub> (Pydc)(Ata) <sub>2</sub>	52.6	35.3	23.6	3.9	15.9	This work

<sup>a</sup> at 296 K.

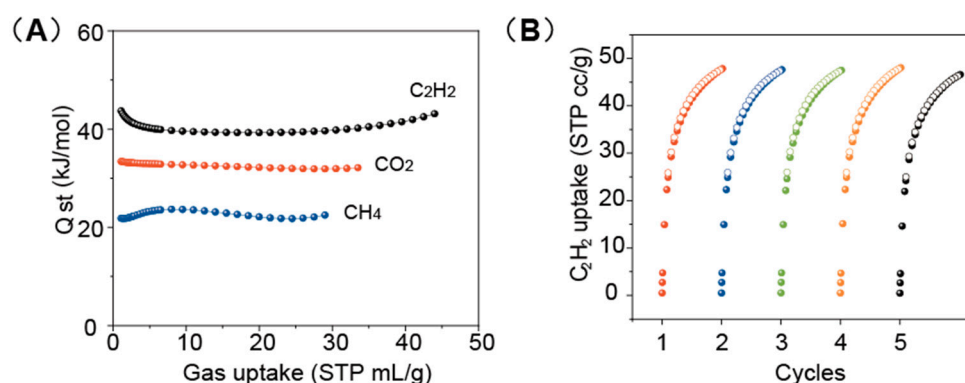


**Figure 4.** (A)  $Q_{st}$  for  $C_2H_2$ ,  $CO_2$  and  $CH_4$  in **1**. (B) Cycling adsorption-desorption experiments. Before every measurement, **1** was regenerated at 200 (1st), 150 (2nd), 100 (3rd) 50 (4th), 25 (5th) °C, respectively, for 30 min.

To further evaluate the dynamic separation of  $C_2H_2/CO_2$  gas mixture, breakthrough experiments were conducted in which an equimolar  $C_2H_2/CO_2$  mixture was flowed over a packed bed of **1** with a total flow of 2 mL/min at 298 K. Figure 5A shows the breakthrough curves of **1** for  $C_2H_2/CO_2$ . Compared with  $C_2H_2$ ,  $CO_2$  eluted first, which could be explained by the favorable affinity of **1** for  $C_2H_2$ , in agreement with the single-component adsorption isotherms in Figure 2D. The typical roll-up of the  $CO_2$  curves also revealed the weaker affinity of **1** for  $CO_2$ . The regeneration of **1** with Ar purge was also studied. At 100 °C and with a Ar flowrate of 3 mL/min, nearly all of the adsorbed  $C_2H_2$  and  $CO_2$  can be blown out within 3 h. These experiments confirmed the excellent potential of **1** for practical separation of  $C_2H_2/CO_2$  mixtures as well as the facile regeneration conditions of the material for consecutive use.

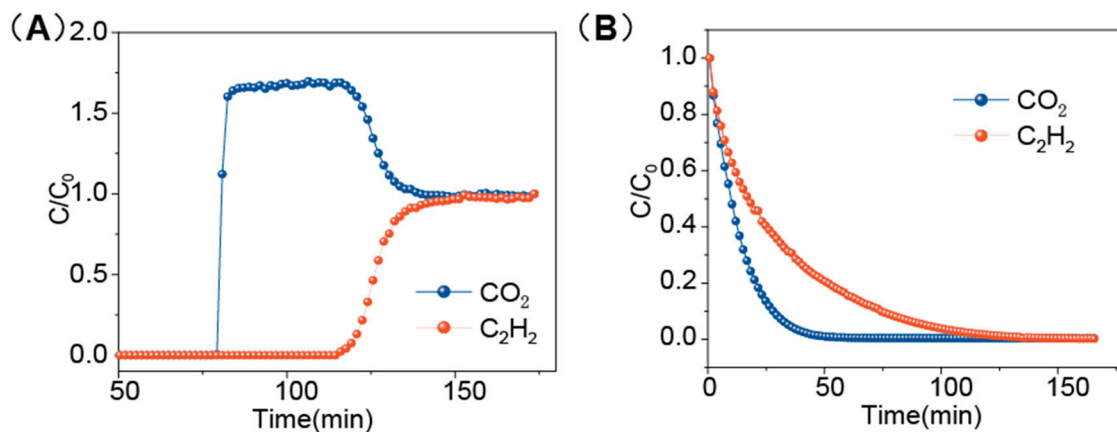


**Figure 5.** (A) Column breakthrough experiments of  $C_2H_2/CO_2$  separation in **1** with a total flowrate of 2 mL/min at 25 °C. (B) Regeneration of **1** using an Ar purge of at 100 °C with a flow rate of 3 mL/min.

### 3. Materials and Methods

#### 3.1. Materials

All the materials were used as received without further purification. Zinc nitrate hexahydrate [ $Zn(NO_3)_2 \cdot 6H_2O$ ], (98% purity) was purchased from Sinopharm (Shanghai, China). 3,5-Pyridinedicarboxylic acid [ $H_2Pydc$ ] (98% purity) and 3-amino-1,2,4-triazole [ $HAta$ ] (99% purity) were purchased from Energy Chemical (Shanghai, China). *N,N*-Dimethylformamide [ $HCON(CH_3)_2$ ] (99.5% purity) was purchased from Chinasun Speciality Products Co. (Jinhua, China).

### 3.2. Synthesis of $Zn_2(Pydc)(Ata)_2$ 1

The method for the small scale synthesis of **1** in an autoclave can be found in reference [38] and is summarized here. To a 25 mL autoclave were added 148.7 mg (0.5 mmol) of  $Zn(NO_3)_2 \cdot 6H_2O$ , 42.0 mg (0.5 mmol) of HAta, 83.6 mg (0.5 mmol) of  $H_2Pydc$ , followed by a stir bar. Then 12 mL of DMF and 1 mL of  $H_2O$  were added. The mixture was stirred under room temperature for 10 min whereupon almost all of the solid was dissolved. Then the stir bar was removed and the autoclave was heated to 100 °C and kept at this temperature for 72 h. When cooled to room temperature, slightly yellow crystals were obtained. Then the crystals were collected by filtration, washed with DMF (3 mL  $\times$  2) and dried under vacuum at 60 °C for 24 h. According to [38], the obtained solid product has a composition of  $Zn_2(Pydc)(Ata)_2 \cdot DMF \cdot 2H_2O$ . Only by heating at 200 °C under high vacuum can the solvent guest molecules in the pores be removed.

For the 1 g synthesis of  $Zn_2(Pydc)(Ata)_2$  the following procedure was performed: A 250 mL round-bottomed flask was charged with  $Zn(NO_3)_2 \cdot 6H_2O$  (1.785 g, 6 mmol), HAta (504.5 mg, 6 mmol) and  $H_2Pydc$  (1.003 g, 6 mmol) and a stir bar. Then 144 mL of DMF and 12 mL of  $H_2O$  were added and the mixture was stirred at 25 °C for about 10 min. Then, the flask bottle was equipped with a condenser, the stirring bar was taken out and the temperature of the oil bath was raised to 100 °C and the heating continued for 72 h. After that, the oil bath was removed, and the round-bottomed flask was allowed to cool to ambient temperature. The resulting powder was collected by filtration, washed with DMF (30 mL), and dried under vacuum at 60 °C for 24 h. The weight after workup was 1.0 g with a yield of 29% based on  $Zn(NO_3)_2 \cdot 6H_2O$ .

For the 10 g synthesis of  $Zn_2(Pydc)(Ata)_2$  without increasing the solvent amount a 250 mL round-bottom flask was charged with  $Zn(NO_3)_2 \cdot 6H_2O$  (10.11 g, 34 mmol), HAta (2.86 g, 34 mmol) and  $H_2Pydc$  (5.68 g, 34 mmol) and a stir bar. 144 mL of DMF and 12 mL of  $H_2O$  were added, and the mixture was stirred at 25 °C for about 10 min. Then, the temperature of the oil bath was raised to 100 °C. The flask was equipped with a condenser and the heating was continued for 72 h. The stir bar was not removed for improving the reaction efficiency as the substrate concentrations on this scale were much higher. After that, the oil bath was removed and the flask was allowed to cool to ambient temperature. The resulting powder was collected by filtration and washed with DMF (15 mL  $\times$  6). During the washing process, two different kinds of solid with different density were observed and separated. One was white (lower density) and the other was slightly yellow (higher density). After analysis, the white one was found to be  $H_2Pydc$ , while the slightly yellow one was product with > 95% purity (see Figure S2). Both solids were dried under vacuum at 60 °C for 24 h. The weights of recovered  $H_2Pydc$  and yellow product were 2.96 g and 4.33 g, respectively. The yield was 45% based on  $Zn(NO_3)_2 \cdot 6H_2O$ .

Using the improved ratio of starting materials an optimized 10 g synthesis of  $Zn_2(Pydc)(Ata)_2$  was performed as follows: A 250 mL round-bottomed flask was charged with  $Zn(NO_3)_2 \cdot 6H_2O$  (10.11 g, 34 mmol), HAta (2.86 g, 34 mmol) and  $H_2Pydc$  (2.84 g, 17 mmol) and a stir bar. 144 mL of DMF and 12 mL of  $H_2O$  were added, and the mixture was stirred at 25 °C for about 10 min. Then, the flask was equipped with a condenser, the temperature of the oil bath was raised to 100 °C and the heating was continued for 72 h. After that, the oil bath was removed, and the flask was allowed to cool to ambient temperature. The resulting powder was collected by filtration, washed with DMF (15 mL  $\times$  6), and dried under vacuum at 60 °C for 24 h. The weight after workup was 8.62 g with a yield of 89% based on  $Zn(NO_3)_2 \cdot 6H_2O$ .

### 3.3. Characterization

Powder X-ray diffraction (PXRD) data were collected on an AXS D8-Advance diffractometer (Bruker, Ettlingen, Germany) ( $Cu\ K\alpha\lambda = 1.540598\ \text{Å}$ ) with an operating power of 40 KV, 30 mA and a scan speed of 4.0°/min. The range of  $2\theta$  was from 5° to 50°.

### 3.4. Adsorption Measurements

The gas adsorption measurements were performed on an Autosorb iQ instrument (Quantachrome, Florida, USA). Before gas adsorption measurements, fresh **1** was evacuated at 200 °C for 12 h until the pressure dropped below 7 μmHg. The adsorption isotherms of C<sub>2</sub>H<sub>2</sub>, CO<sub>2</sub>, and CH<sub>4</sub> were all collected at 278, 288, and 298 K on activated samples.

### 3.5. Calculation for Adsorption Selectivity and Isotheric Heat of Adsorption

The adsorption isotherms in **1** were fitted using a dual-site Langmuir-Freundlich model:

$$q = q_{A, \text{sat}} \frac{b_A p^{v_A}}{1 + b_A p^{v_A}} + q_{B, \text{sat}} \frac{b_B p^{v_B}}{1 + b_B p^{v_B}} \quad (1)$$

Here,  $p$  (unit: kPa) is the pressure of the bulk gas at equilibrium with the adsorbed phase,  $q$  (unit: L kg<sup>-1</sup>) is the adsorbed gas volume per mass of adsorbent,  $q_{A, \text{sat}}$  and  $q_{B, \text{sat}}$  (unit: L kg<sup>-1</sup>) are the saturation capacities of site A and B,  $b_A$  and  $b_B$  (unit: kPa<sup>-v</sup>) are the affinity coefficients of site A and B, and  $v_A$  and  $v_B$  represent the deviations from an ideal homogeneous surface.

The isotheric heat of adsorption,  $Q_{\text{st}}$ , is calculated based on the Clausius-Clapeyron equation:

$$Q_{\text{st}} = RT^2 \left( \frac{\partial \ln p}{\partial T} \right)_q \quad (2)$$

The IAST adsorption selectivity for two gases is defined as:

$$S_{\text{ads}} = \frac{q_1/p_1}{q_2/p_2} \quad (3)$$

where  $q_1$ , and  $q_2$  are the equilibrium gas uptake from the adsorbed phase with partial pressures  $p_1$ , and  $p_2$

### 3.6. Breakthrough Experiments

The breakthrough experiment was conducted at 298 K on a self-constructed separation setup equipped with a stainless steel column (Φ 4.6 mm × 100 mm). The weight of activated **1** packed in the column was 1.6913 g. The column packed with sample was first purged with a Ar flow (10 mL min<sup>-1</sup>) for 12 h at 100 °C for activation. A C<sub>2</sub>H<sub>2</sub>/CO<sub>2</sub> = 1/1 (v/v) gas mixture was then introduced at 2 mL min<sup>-1</sup>. The flow rates of gases were regulated by mass flow controllers and outlet gas concentration was monitored by gas chromatography (GC-9860-5CNJ, Hope, Nanjing, China) using a thermal conductivity detector (TCD) with a detection limit of 100 ppm). After the breakthrough experiment, the column was regenerated with an Ar flow (3 mL min<sup>-1</sup>) at 100 °C for 5 h.

## 4. Conclusions

In conclusion, a large-scale synthetic route to Zn<sub>2</sub>(Pydc)(Ata)<sub>2</sub> (**1**), a highly water and thermally stable MOF, was reported. The synthesized material was used in the separation of C<sub>2</sub>H<sub>2</sub> from CH<sub>4</sub> and CO<sub>2</sub> with relatively high IAST selectivities for equimolar C<sub>2</sub>H<sub>2</sub>/CO<sub>2</sub> (5.1) and C<sub>2</sub>H<sub>2</sub>/CH<sub>4</sub> (21.5) gas mixtures, respectively, comparable to those of many popular MOFs. The practical separation performance for C<sub>2</sub>H<sub>2</sub>/CO<sub>2</sub> mixture was confirmed by dynamic breakthrough experiments. In addition, **1** can be easily regenerated by vacuum or Ar purging, underscoring its potential use for C<sub>2</sub>H<sub>2</sub>/CO<sub>2</sub> (5.1) and C<sub>2</sub>H<sub>2</sub>/CH<sub>4</sub> (21.5) separation in industry.

**Supplementary Materials:** The following are available online. Figure S1: Photographs illustrating the reaction process, Figure S2: PXRD patterns comparison, Table S1: Langmuir-Freundlich parameters fit for C<sub>2</sub>H<sub>2</sub>, CO<sub>2</sub>, and CH<sub>4</sub> in Zn<sub>2</sub>(Pydc)(Ata)<sub>2</sub> at 298 K, Table S2: Langmuir-Freundlich parameters fit for C<sub>2</sub>H<sub>2</sub>, CO<sub>2</sub>, and CH<sub>4</sub> in Zn<sub>2</sub>(Pydc)(Ata)<sub>2</sub> at 288 K, Table S3: Langmuir-Freundlich parameters fit for C<sub>2</sub>H<sub>2</sub>, CO<sub>2</sub>, and CH<sub>4</sub> in Zn<sub>2</sub>(Pydc)(Ata)<sub>2</sub> at 278 K.



**Author Contributions:** Conceptualization, Y.Z.; Methodology, N.X., Y.J. (Yunjia Jiang), W.S.; Validation, J.L., Y.J. (Yujie Jin); Formal Analysis, N.X., Y.J. (Yunjia Jiang), W.S.; Writing–Original Draft Preparation, N.X., Y.Z.; Writing–Review & Editing, Y.J. (Yunjia Jiang), L.W., Y.Z., S.D.; Supervision, Y.Z., D.W., S.D.; Funding Acquisition, L.W., Y.Z., S.D. All authors have read and agreed to the published version of the manuscript.

**Funding:** This research was funded by the National Natural Science Foundation of China (No. 21908193, 21871231, 21850410451), the Special Funds for Basic Scientific Research of Zhejiang University.

**Institutional Review Board Statement:** Not applicable.

**Informed Consent Statement:** Not applicable.

**Data Availability Statement:** The data that support the findings of this study are available in the Supplementary Materials of this article or from the corresponding author upon reasonable request.

**Conflicts of Interest:** The authors declare no conflict of interest.

**Sample Availability:** Samples of the compounds are not available from the authors.

## References

1. Stang, P.J.; Diederich, F. *Modern Acetylene Chemistry*; WileyVCH: Weinheim, Germany, 2008.
2. Alduhaish, O.; Wang, H.; Li, B.; Hu, T.-L.; Arman, H.D.; Alfooty, K.; Chen, B. A Twofold Interpenetrated Metal–Organic Framework with High Performance in Selective Separation of C<sub>2</sub>H<sub>2</sub>/CH<sub>4</sub>. *ChemPlusChem* **2016**, *81*, 770–774. [[CrossRef](#)]
3. Zhang, L.; Jiang, K.; Li, Y.; Zhao, D.; Yang, Y.; Cui, Y.; Chen, B.; Qian, G. Microporous Metal–Organic Framework with Exposed Amino Functional Group for High Acetylene Storage and Excellent C<sub>2</sub>H<sub>2</sub>/CO<sub>2</sub> and C<sub>2</sub>H<sub>2</sub>/CH<sub>4</sub> Separations. *Cryst. Growth Des.* **2017**, *17*, 2319–2322. [[CrossRef](#)]
4. Hou, X.-J.; He, P.; Li, H.; Wang, X. Understanding the Adsorption Mechanism of C<sub>2</sub>H<sub>2</sub>, CO<sub>2</sub>, and CH<sub>4</sub> in Isostructural Metal–Organic Frameworks with Coordinatively Unsaturated Metal Sites. *J. Phys. Chem. C* **2013**, *117*, 2824–2834. [[CrossRef](#)]
5. Sholl, D.S.; Lively, R.P. Seven chemical separations to change the world. *Nature* **2016**, *532*, 435–438. [[CrossRef](#)]
6. Zhang, Y.; Hu, J.; Krishna, R.; Wang, L.; Yang, L.; Cui, X.; Duttwyler, S.; Xing, H. Rational Design of Microporous MOFs with Anionic Boron Cluster Functionality and Cooperative Dihydrogen Binding Sites for Highly Selective Capture of Acetylene. *Angew. Chem. Int. Ed.* **2020**, *59*, 17664–17669. [[CrossRef](#)] [[PubMed](#)]
7. Zhao, X.; Wang, Y.; Li, D.S.; Bu, X.; Feng, P. Metal–Organic Frameworks for Separation. *Adv. Mater.* **2018**, *30*, 1705189. [[CrossRef](#)] [[PubMed](#)]
8. Bao, Z.; Chang, G.; Xing, H.; Krishna, R.; Ren, Q.; Chen, B. Potential of microporous metal–organic frameworks for separation of hydrocarbon mixtures. *Energy Environ. Sci.* **2016**, *9*, 3612–3641. [[CrossRef](#)]
9. Liao, P.-Q.; Huang, N.-Y.; Zhang, W.-X.; Zhang, J.-P.; Chen, X.-M. Controlling guest conformation for efficient purification of butadiene. *Science* **2017**, *356*, 1193–1196. [[CrossRef](#)]
10. Li, Y.-P.; Wang, Y.; Xue, Y.-Y.; Li, H.-P.; Zhai, Q.-G.; Li, S.-N.; Jiang, Y.-C.; Hu, M.-C.; Bu, X. Ultramicroporous Building Units as a Path to Bi-microporous Metal–Organic Frameworks with High Acetylene Storage and Separation Performance. *Angew. Chem. Int. Ed.* **2019**, *58*, 13590–13595. [[CrossRef](#)]
11. Lin, S.; Zhou, P.; Xu, T.; Fan, L.; Wang, X.; Yue, L.; Jiang, Z.; Zhang, Y.; Zhang, Z.; He, Y. Modulation of Topological Structures and Adsorption Properties of Copper-Tricarboxylate Frameworks Enabled by the Effect of the Functional Group and Its Position. *Inorg. Chem.* **2021**, *60*, 8111–8122. [[CrossRef](#)]
12. Qiao, J.; Liu, X.; Liu, X.; Zhang, L.; Liu, Y. Two urea-functionalized pcu metal-organic frameworks based on a pillared-layer strategy for gas adsorption and separation. *Inorg. Chem. Front.* **2020**, *7*, 3500–3508. [[CrossRef](#)]
13. Hua, G.-F.; Xie, X.-J.; Lu, W.-G.; Li, D. Optimizing supramolecular interactions in metal-organic frameworks for C<sub>2</sub> separation. *Dalton Trans.* **2020**, *49*, 15548–15559. [[CrossRef](#)]
14. Wang, Y.; Yuan, S.; Hu, Z.; Kundu, T.; Zhang, J.; Peh, S.B.; Cheng, Y.; Dong, J.; Yuan, D.; Zhou, H.-C.; et al. Pore Size Reduction in Zirconium Metal–Organic Frameworks for Ethylene/Ethane Separation. *ACS Sustain. Chem. Eng.* **2019**, *7*, 7118–7126. [[CrossRef](#)]
15. Peng, Y.-L.; Pham, T.; Li, P.; Wang, T.; Chen, Y.; Chen, K.-J.; Forrest, K.A.; Space, B.; Cheng, P.; Zaworotko, M.J.; et al. Robust Ultramicroporous Metal–Organic Frameworks with Benchmark Affinity for Acetylene. *Angew. Chem. Int. Ed.* **2018**, *57*, 10971–10975. [[CrossRef](#)]
16. Jiang, Z.; Zou, Y.; Xu, T.; Fan, L.; Zhou, P.; He, Y. A Hydrostable Cage-Based MOF with Open Metal Sites and Lewis Basic Sites Immobilized in Pore Surface for Efficient Separation and Purification of Natural Gas and C<sub>2</sub>H<sub>2</sub>. *Dalton Trans.* **2020**, *49*, 3553–3561. [[CrossRef](#)]
17. Xu, T.; Fan, L.; Jiang, Z.; Zhou, P.; Li, Z.; Lu, H.; He, Y. Immobilization of N-Oxide Functionality into Nbo-Type Mofs for Significantly Enhanced C<sub>2</sub>H<sub>2</sub>/CH<sub>4</sub> and CO<sub>2</sub>/CH<sub>4</sub> Separations. *Dalton Trans.* **2020**, *49*, 7174–7181. [[CrossRef](#)]
18. Li, N.; Chang, Z.; Huang, H.; Feng, R.; He, W.-W.; Zhong, M.; Madden, D.G.; Zaworotko, M.-J.; Bu, X.-H. Specific K<sup>+</sup> Binding Sites as CO<sub>2</sub> Traps in a Porous MOF for Enhanced CO<sub>2</sub> Selective Sorption. *Small* **2019**, *15*, 1900426. [[CrossRef](#)]

19. Kumar, A.; Madden, D.G.; Lusi, M.; Chen, K.-J.; Daniels, E.A.; Curtin, T.; Perry, J.J., IV; Zaworotko, M.J. Direct Air Capture of CO<sub>2</sub> by Physisorbent Materials. *Angew. Chem. Int. Ed.* **2015**, *54*, 14372–14377. [[CrossRef](#)]
20. Song, X.; Zhang, M.; Duan, J.; Bai, J. Constructing and finely tuning the CO<sub>2</sub> traps of stable and various-pore-containing MOFs towards highly selective CO<sub>2</sub> capture. *Chem. Commun.* **2019**, *55*, 3477–3480. [[CrossRef](#)]
21. Ma, H.-Y.; Zhang, Y.-Z.; Yan, H.; Zhang, W.-J.; Li, Y.-W.; Wang, S.-N.; Li, D.-C.; Dou, J.-M.; Li, J.-R. Two microporous CoII-MOFs with dual active sites for highly selective adsorption of CO<sub>2</sub>/CH<sub>4</sub> and CO<sub>2</sub>/N<sub>2</sub>. *Dalton Trans.* **2019**, *48*, 13541–13545. [[CrossRef](#)]
22. Chen, Y.; Wu, H.; Xiao, Q.; Lv, D.; Li, F.; Li, Z.; Xia, Q. Rapid room temperature conversion of hydroxy double salt to MOF-505 for CO<sub>2</sub> capture. *Cryst. Eng. Comm.* **2019**, *21*, 165–171. [[CrossRef](#)]
23. Zhang, Y.; Cui, X.; Xing, H. Recent advances in the capture and abatement of toxic gases and vapors by metal-organic frameworks. *Mater. Chem. Front.* **2021**, *5*, 5970–6013. [[CrossRef](#)]
24. Moon, S.-Y.; Liu, Y.; Hupp, J.T.; Farha, O.K. Instantaneous Hydrolysis of Nerve-Agent Simulants with a Six-Connected Zirconium-Based Metal-Organic Framework. *Angew. Chem. Int. Ed.* **2015**, *54*, 6795–6799. [[CrossRef](#)] [[PubMed](#)]
25. Sabyrov, K.; Jiang, J.; Yaghi, O.M.; Somorjai, G.A. Hydroisomerization of n-Hexane Using Acidified Metal–Organic Framework and Platinum Nanoparticles. *J. Am. Chem. Soc.* **2017**, *139*, 12382–12385. [[CrossRef](#)] [[PubMed](#)]
26. Niu, Z.; Zhang, W.; Lan, P.C.; Aguila, B.; Ma, S. Promoting Frustrated Lewis Pairs for Heterogeneous Chemoselective Hydrogenation via the Tailored Pore Environment within Metal-Organic Frameworks. *Angew. Chem. Int. Ed.* **2019**, *58*, 7420–7424. [[CrossRef](#)]
27. Yue, D.; Zhao, D.; Zhang, J.; Zhang, L.; Jiang, K.; Zhang, X.; Cui, Y.; Yang, Y.; Chen, B.; Qian, G. A luminescent cerium metal-organic framework for the turn-on sensing of ascorbic acid. *Chem. Commun.* **2017**, *53*, 11221–11224. [[CrossRef](#)]
28. Han, X.; Gu, C.; Ding, Y.; Yu, J.; Li, K.; Zhao, D.; Chen, B. Stable Eu<sup>3+</sup>/Cu<sup>2+</sup>-Functionalized Supramolecular Zinc(II) Complexes as Fluorescent Probes for Turn-On and Ratiometric Detection of Hydrogen Sulfide. *ACS Appl. Mater. Interfaces* **2021**, *13*, 20371–20379. [[CrossRef](#)]
29. Jiang, J.; Furukawa, H.; Zhang, Y.-B.; Yaghi, O.M. High Methane Storage Working Capacity in Metal–Organic Frameworks with Acrylate Links. *J. Am. Chem. Soc.* **2016**, *138*, 10244–10251. [[CrossRef](#)] [[PubMed](#)]
30. Wang, H.Y.; Ye, W.Q.; Yang, Y.; Zhong, Y.; Hu, Y. Zn-ion hybrid supercapacitors: Achievements, challenges and future perspectives. *Nano Energy* **2021**, *85*, 105942. [[CrossRef](#)]
31. Hanikel, N.; Prevot, M.S.; Yaghi, O.M. MOF water harvesters. *Nat. Nanotechnol.* **2020**, *15*, 348–355. [[CrossRef](#)] [[PubMed](#)]
32. Pei, J.; Shao, K.; Wang, J.-X.; Wen, H.-M.; Yang, Y.; Cui, Y.; Krishna, R.; Li, B.; Qian, G. A Chemically Stable Hofmann-Type Metal–Organic Framework with Sandwich-Like Binding Sites for Benchmark Acetylene Capture. *Adv. Mater.* **2020**, *32*, 1908275. [[CrossRef](#)]
33. Niu, Z.; Cui, X.; Pham, T.; Verma, G.; Lan, P.C.; Shan, C.; Xing, H.; Forrest, K.A.; Suepaul, S.; Space, B.; et al. A MOF-based Ultra-Strong Acetylene Nano-trap for Highly Efficient C<sub>2</sub>H<sub>2</sub>/CO<sub>2</sub> Separation. *Angew. Chem. Int. Ed.* **2021**, *60*, 5283–5288. [[CrossRef](#)]
34. Wang, L.; Jiang, T.; Duttwyler, S.; Zhang, Y. Supramolecular Cu(II)-dipyridyl frameworks featuring weakly coordinating dodecaborate dianions for selective gas separation. *Cryst. Eng. Comm.* **2021**, *23*, 282–291. [[CrossRef](#)]
35. Wang, L.; Sun, W.; Duttwyler, S.; Zhang, Y. Efficient adsorption separation of methane from CO<sub>2</sub> and C<sub>2</sub>–C<sub>3</sub> hydrocarbons in a microporous closo-dodecaborate [B<sub>12</sub>H<sub>12</sub>]<sup>2−</sup> pillared metal-organic framework. *J. Solid State Chem.* **2021**, *299*, 122167. [[CrossRef](#)]
36. Yang, L.; Cui, X.; Zhang, Y.; Wang, Q.; Zhang, Z.; Suo, X.; Xing, H. Anion Pillared Metal–Organic Framework Embedded with Molecular Rotors for Size-Selective Capture of CO<sub>2</sub> from CH<sub>4</sub> and N<sub>2</sub>. *ACS Sustain. Chem. Eng.* **2019**, *7*, 3138–3144. [[CrossRef](#)]
37. Lin, R.-B.; Li, L.; Zhou, H.-L.; Wu, H.; He, C.; Li, S.; Krishna, R.; Li, J.; Zhou, W.; Chen, B. Molecular sieving of ethylene from ethane using a rigid metal-organic framework. *Nat. Mater.* **2018**, *17*, 1128–1133. [[CrossRef](#)] [[PubMed](#)]
38. Lan, J.; Qu, Y.; Zhang, X.; Ma, H.; Xu, P.; Sun, J. A novel water-stable MOF Zn(Py)(Atz) as heterogeneous catalyst for chemical conversion of CO<sub>2</sub> with various epoxides under mild conditions. *J. CO<sub>2</sub> Util.* **2020**, *35*, 216–224. [[CrossRef](#)]
39. Zhang, Y.; Yang, L.; Wang, L.; Duttwyler, S.; Xing, H. A Microporous Metal-Organic Framework Supramolecularly Assembled from a Cu(II) Dodecaborate Cluster Complex for Selective Gas Separation. *Angew. Chem. Int. Ed.* **2019**, *58*, 8145–8150. [[CrossRef](#)]
40. Xu, T.; He, M.; Fan, L.; Zhou, P.; Jiang, Z.; He, Y. Engineering ligand conformation by substituent manipulation towards diverse copper-tricarboxylate frameworks with tuned gas adsorption properties. *Dalton Trans.* **2021**, *50*, 638–646. [[CrossRef](#)]
41. Zhang, Y.; Yang, L.; Wang, L.; Cui, X.; Xing, H. Pillar iodination in functional boron cage hybrid supramolecular frameworks for high performance separation of light hydrocarbons. *J. Mater. Chem. A* **2019**, *7*, 27560–27566. [[CrossRef](#)]
42. Chang, G.; Li, B.; Wang, H.; Hu, T.; Bao, Z.; Chen, B. Control of interpenetration in a microporous metal–organic framework for significantly enhanced C<sub>2</sub>H<sub>2</sub>/CO<sub>2</sub> separation at room temperature. *Chem. Commun.* **2016**, *52*, 3494–3496. [[CrossRef](#)]
43. Li, L.; Yin, Q.; Li, H.-F.; Liu, T.-F.; Cao, R. Rational design of phosphonocarboxylate metal–organic frameworks for light hydrocarbon separations. *Mater. Chem. Front.* **2018**, *2*, 1436–1440. [[CrossRef](#)]
44. Fan, L.; Lin, S.; Wang, X.; Yue, L.; Xu, T.; Jiang, Z.; He, Y. A Series of Metal–Organic Framework Isomers Based on Pyridinedicarboxylate Ligands: Diversified Selective Gas Adsorption and the Positional Effect of Methyl Functionality. *Inorg Chem.* **2021**, *60*, 2704–2715. [[CrossRef](#)]
45. Das, M.C.; Xu, H.; Xiang, S.; Zhang, Z.; Arman, H.D.; Qian, G.; Chen, B. A New Approach to Construct a Doubly Interpenetrated Microporous Metal–Organic Framework of Primitive Cubic Net for Highly Selective Sorption of Small Hydrocarbon Molecules. *Chem. Eur. J.* **2011**, *17*, 7817–7822. [[CrossRef](#)]

46. Ding, T.; Zhang, S.; Zhang, W.; Zhang, G.; Gao, Z.W. Highly selective C<sub>2</sub>H<sub>2</sub> and CO<sub>2</sub> capture and magnetic properties of robust Co-chain based metal–organic framework. *Dalton Trans.* **2019**, *48*, 7938–7945. [[CrossRef](#)]
47. Lin, R.-G.; Lin, R.-B.; Chen, B. A microporous metal–organic framework for selective C<sub>2</sub>H<sub>2</sub> and CO<sub>2</sub> Separation. *J. Solid State Chem.* **2017**, *252*, 138–141. [[CrossRef](#)]
48. Huang, P.; Chen, C.; Wu, M.; Jiang, F.; Hong, M. An indium-organic framework for efficient storage of light hydrocarbons and selective removal of organic dyes. *Dalton Trans.* **2019**, *48*, 5527–5533. [[CrossRef](#)]
49. Zeng, H.; Xie, M.; Huang, Y.L.; Zhao, Y.; Xie, X.J.; Bai, J.P.; Wan, M.Y.; Krishna, R.; Lu, W.; Li, D. Induced Fit of C<sub>2</sub>H<sub>2</sub> in a Flexible MOF Through Cooperative Action of Open Metal Sites. *Angew. Chem. Int. Ed.* **2019**, *58*, 8515–8519. [[CrossRef](#)]
50. Liu, R.; Liu, Q.Y.; Krishna, R.; Wang, W.; He, C.T.; Wang, Y.L. Water-Stable Europium 1,3,6,8-Tetrakis(4-carboxylphenyl)pyrene Framework for Efficient C<sub>2</sub>H<sub>2</sub>/CO<sub>2</sub> Separation. *Inorg. Chem.* **2019**, *58*, 5089–5095. [[CrossRef](#)]
51. Liu, L.; Yao, Z.; Ye, Y.; Chen, L.; Lin, Q.; Yang, Y.; Zhang, Z.; Xiang, S. Robustness, Selective Gas Separation, and Nitrobenzene Sensing on Two Isomers of Cadmium Metal–Organic Frameworks Containing Various Metal–O–Metal Chains. *Inorg. Chem.* **2018**, *57*, 12961–12968. [[CrossRef](#)]
52. Wang, L.; Sun, W.; Zhang, Y.; Xu, N.; Krishna, R.; Hu, J.; Jiang, Y.; He, Y.; Xing, H. Interpenetration symmetry control within ultramicroporous robust boron cluster hybrid MOFs for benchmark purification of acetylene from carbon dioxide. *Angew. Chem. Int. Ed.* **2021**. [[CrossRef](#)]
53. Li, Y.T.; Zhang, J.W.; Lv, H.J.; Hu, M.C.; Li, S.N.; Jiang, Y.C.; Zhai, Q.G. Tailoring the Pore Environment of a Robust Ga-MOF by Deformed [Ga<sub>3</sub>O(COO)<sub>6</sub>] Cluster for Boosting C<sub>2</sub>H<sub>2</sub> Uptake and Separation. *Inorg. Chem.* **2020**, *59*, 10368–10373. [[CrossRef](#)] [[PubMed](#)]